# Structure and charge order in the antiferromagnetic band-insulating phase of $NdNiO_3$

J. L. García-Muñoz*
*Institut de Ciència de Materials de Barcelona, CSIC, Campus Universitari de Bellaterra, E-08193 Bellaterra, Barcelona, Spain*

M. A. G. Aranda
*Departamento de Química Inorgánica, Cristalografía y Mineralogía, Universidad de Málaga, 29071 Málaga, Spain*

J. A. Alonso and M. J. Martínez-Lope
*Instituto de Ciencia de Materiales de Madrid, CSIC, Cantoblanco, E-28049 Madrid, Spain*

(Received 11 January 2009; published 28 April 2009)

We present a high-resolution synchrotron powder-diffraction investigation on $NdNiO_3$ that confirms the presence on long-range charge order below the metal-insulator transition previously reported at $T_{MI}=205$ K. The monoclinic symmetry of the insulating state is unambiguously proved. A detailed description of the true crystal structure in the antiferromagnetic phase ($T_{MI}=T_N$) was obtained that proves the occurrence of two octahedral sites below $T_{MI}$. Antiferromagnetic $NdNiO_3$ presents long-range charge order with $\delta \approx 0.2-0.3 \ll 1$. The breathing distortion observed in the octahedra reduces the repulsion $U$ at Ni sites, avoids Jahn-Teller effect, and allows charge segregation. The phonon-assisted partial charge disproportionation is a common mechanism in $RNiO_3$ oxides. With the exception of $LaNiO_3$, the compounds of the whole family of $RNiO_3$ perovskites must be considered band insulators with a charge ordered ground state at low temperature.

DOI: 10.1103/PhysRevB.79.134432 PACS number(s): 71.30.+h, 71.45.Lr

The unconventional electronic and magnetic properties of the nickel perovskites $RNiO_3$ ($R$: rare-earth) have been the object of extensive investigations.[1–12] A sharp insulator-to-metal transition occurs at a temperature that increases as the ionic radii of the lanthanide ion is reduced.[1–3] In these oxides the transformation from localized electron into delocalized electron states can be induced by temperature, chemical, or hydrostatic pressure,[13–15] and it is in great contrast with the Mott transition in more conventional oxides. Initially, the metal-to-insulator transition at $T_{MI}$ was attributed to a charge transfer gap due to bandwidth narrowing.[2,3,5] The reported magnetic order in the insulating phase suggested an orbital ordered state.[5–7] But several works demonstrated the absence of orbital or Jahn-Teller (JT) order.[6,9,16] It was then apparent that any of these two common mechanisms in narrow band oxides were breaking down the twofold degeneracy of the singly occupied $e_g$ orbital [in the low spin $Ni^{3+}(t_{2g}^6 e_g^1)$ state].

The scenario changed after the detection of a subtle symmetry change in $YNiO_3$ signaling charge order in the insulating phase.[17] Charge disproportionation and a subtle symmetry change from orthorhombic to monoclinic was unambiguously observed at the metal-insulator transition in the heaviest rare-earth nickelates ($RNiO_3$, from Y to Lu, the smallest member of the family).[17–19] These perovskites with simple structure are very attractive examples of how orbital degeneracy can be lifted through charge ordering instead of Jahn-Teller distortion if the system is close to the itinerant state boundary.[17,20] This mechanism is based on charge segregation and does not require orbital ordering. It is driven by the Hund's coupling and is favored by a limited delocalization of the $e_g$ electrons (a certain band broadening that transforms the levels into bands).[20] $AgNiO_2$ has been shown to be a 2D analog to $RNiO_3$ (Ref. 21).

After the discovery of long-range-ordered charge segregation in heavy $RNiO_3$ perovskites (from Y to Lu) many efforts were made to detect charge disproportionation (long- or short-ranged) in $RNiO_3$ compounds of large rare-earth cations (light rare earths). The coexistence of contracted/expanded $NiO_6$ octahedra in the compounds with lighter (from Dy to Pr) lanthanides is a long-standing open question, given that the difficulties for detecting the expected symmetry breaking at $T_{MI}$ increase extraordinarily for large rare earths. At present, some available results are contradictory. Neutron-diffraction studies across $T_{MI}$ were reported in Ref. 3 for $R$=La, Pr and Nd, and in Ref. 9 for Sm and Eu. They did not detect symmetry changes, and using the *Pbnm* description, an isotropic expansion of the cell and the Ni-O bonds ($\Delta d_{Ni\text{-}O} \approx +0.004$ Å) was reported across the transition.[3] A crossover in the nature of the metallic phases has been proposed by several groups on moving from heavy to light $RNiO_3$ nickelates.[22–24] On the other hand, recent Raman spectra, electron diffraction,[25] and resonant x-ray scattering[26] on $NdNiO_3$ thin films were compatible with an orthorhombic-to-monoclinic transition. Moreover, from a x-ray-absorption study of $PrNiO_3$ and $NdNiO_3$, Piamonteze *et al.*[27] concluded that the insulating phase of these compounds presents two different Ni sites and charge order, at least at the short-range scale. Some examples of challenging issues in slightly distorted $RNiO_3$ perovskites are (1) rule out or confirm a possible phase boundary in the origin of the insulator state on going from the small to the large rare-earth cations nickelates; (2) distinguish between the possibility of two different Ni sites organized in short-range or long-range charge order, (3) provide a correct detailed structural description that permit the comparison with the smaller members of the family; (4) quantum critical characteristics in their $T$-$P$ phase diagram. In this work we have tried to give answer to the first three questions. We present a high-resolution synchrotron diffraction study on $NdNiO_3$ that has permitted us to obtain its true insulating structure. After several attempts, it is the first time that its low-temperature distorted structure is properly described.

 

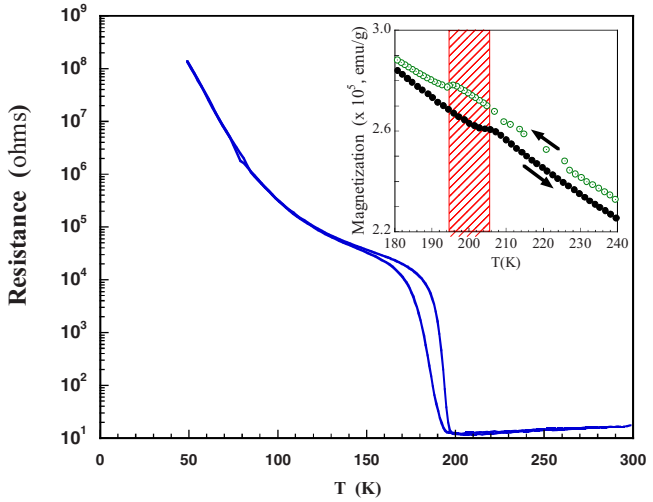


FIG. 1. (Color online) Resistance of $NdNiO_3$ (on heating and cooling) showing an augment of 3 orders of magnitude after formation of a charge order phase. Inset: kink in the susceptibility related with the metal-insulator transition and the onset of the antiferromagnetic order ($T_N=T_{MI}$). Hysteresis on heating and cooling can be appreciated.

Polycrystalline $NdNiO_3$ was synthesized under high oxygen pressure (200 bar) following the procedure described in Ref. 28. The sample was extensively characterized by laboratory x-ray powder diffraction, magnetic and electric measurements, and synchrotron diffraction, which confirmed its quality. High-resolution synchrotron x-ray powder-diffraction (SPD) measurements were performed at the ESRF in Grenoble (BM16). Good quality diffraction patterns were collected at 290 and 50 K, using a short wavelength of $\lambda=0.518056(3)$ Å. Polycrystalline $NdNiO_3$ was loaded in a borosilicate glass capillary ($\phi=0.5$ mm) and rotated during data collection. The counting time was about 3 h to have the desired statistics over the angular range 4 to 42 degrees in $2\theta$. The data were analyzed by the Rietveld method using the FULLPROF (Ref. 29) program. A minor residual NiO phase was detected and accounted for appropriately in the refinements.

The electrical resistance shown in Fig. 1 illustrates the abrupt change in the resistance (about 3 orders of magnitude) at the metal-insulator transition, $T_{MI}\approx 205$ K. The hysteretic behavior of the resistivity extends along the interval 110–205 K and suggests a possible coexistence of metallic and insulating phases over that temperature range. Although there is not yet a proper explanation of the change in the spectral properties of $NdNiO_3$ down to temperatures as low as $\approx 0.5T_{MI}$ (Ref. 22), they appear to be related to electronic inhomogeneities in that temperature range. On the contrary, in the compounds with $T_N\neq T_{MI}$ (like $SmNiO_3$ or $EuNiO_3$) no changes were observed in the photoemission spectra below $T_{MI}$ (Ref. 22). Figure 1 also shows the hysteretic small anomaly in the susceptibility $\chi(T)$ at $T_N=T_{MI}$.

Synchrotron diffraction data were collected at both sides of the metal-insulator transition. 50 K is far below the temperature interval with hysteretic behavior of the resistivity. Diffraction data collected a 290 K (metallic phase) were refined using the orthorhombic *Pbnm* symmetry. The room temperature (RT) structure, interatomic distances, and angles reported in Ref. 3 were confirmed. The corresponding atomic coordinates are given in Table I. Selected interatomic distances and angles are shown in Table II, where we have also reproduced for comparison the values reported in Ref. 3 from neutron data using the *Pbnm* group. The high angular resolution of the synchrotron x-ray data allowed us to determine the cell dimensions with high precision. $NdNiO_3$ cell is highly pseudocubic ($a$[=5.3871 Å]$\approx b$[=5.3826 Å] $\approx c/\sqrt{2}$[=5.3807 Å]); it is the member of the $RNiO_3$ family with the highest metric pseudocubicity. This is shown in Fig. 2, where RT cell parameters and the orthorhombic strain obtained for $NdNiO_3$ are compared to those of other nickelates.

TABLE I. (a) Refined atomic coordinates for $NdNiO_3$ at 290 K in space group *Pbnm*. (b) Refined atomic coordinates for $NdNiO_3$ at 50 K in space group $P2_1/n$.

(a) $a=5.38712(2)$, $b=5.38267(2)$, $c=7.60940(3)$ Å

| Atom | $x$ | $y$ | $z$ | $B$ (Å$^2$) |
|---|---|---|---|---|
| Nd (4c) | 0.9958(2) | 0.0350(1) | 1/4 | 0.65(2) |
| Ni (4b) | 1/2 | 0 | 0 | 0.32(2) |
| O1 (4c) | 0.0692(9) | 0.4896(9) | 1/4 | 0.72(8) |
| O2 (8d) | 0.7165(9) | 0.2870(9) | 0.0394(9) | 1.13(9) |

Reliability factors

| 290 K | $\chi^2$ | $R_B$ | $R_f$ |
|---|---|---|---|
| *Pbnm* | 4.53 | 3.06 | 4.81 |

(b) $a=5.37783(5)$, $b=5.38846(4)$, $c=7.60511(6)$ Å, $\beta=90.061(1)°$

| Atom | $x$ | $y$ | $z$ | $B$ (Å$^2$) |
|---|---|---|---|---|
| Nd (4c) | 0.99321(1) | 0.03910(7) | 0.2495(3) | 0.52(2) |
| Ni1 (2d) | 1/2 | 0 | 0 | 0.55(5) |
| Ni2 (2c) | 1/2 | 0 | 1/2 | 0.28(5) |
| O1 (4e) | 0.0752(17) | 0.4866(9) | 0.2521(29) | 0.54(6) |
| O2a (4e) | 0.7143(29) | 0.2762(29) | 0.0267(16) | 0.55(8) |
| O2b (4e) | 0.2187(26) | 0.2036(29) | 0.9470(17) | 0.57(8) |

Reliability factors

| 50 K | $\chi^2$ | $R_B$ | $R_f$ |
|---|---|---|---|
| $P2_1/n$ | 5.07 | 5.26 | 2.93 |

Regarding the insulating phase, we have tested the orthorhombic *Pbnm* and monoclinic $P2_1/n$ symmetries against the data recorded at 50 K (see Fig. 3). Although differences in the reliability factors were not huge, we obtained better fitting indices with the $P2_1/n$ than with the *Pbnm* description: $R_B=5.26(5.59)$ and $\chi^2=5.07(6.60)$ in the refined monoclinic (orthorhombic) model. However, a more direct and definitive evidence of the real symmetry was achieved by visual examination of the high-resolution SPD profile below

TABLE II. Selected bond distances and angles for $NdNiO_3$ in the metallic (290 K) and the insulating (50 K) regimes. Present values are compared to those given in Ref. 3.

| | Insulator | | Metal | |
|---|---|---|---|---|
| | Synchrotron This work 50 K $P2_1/n$ | Neutron Ref. 3 1.5 K *Pbnm* | Synchrotron This work 290 K *Pbnm* | Neutron Ref. 3 300 K *Pbnm* |
| Ni1-O1(Å) | 1.930(16) | 1.942(2) | 1.941(2) | 1.940(2) |
| Ni1-O2(Å) | 1.891(15) | 1.941(4) | 1.928(9) | 1.940(3) |
| Ni1-O3(Å) | 1.911(15) | 1.954(4) | 1.961(9) | 1.947(3) |
| ⟨Ni1-O⟩(Å) | 1.910 | 1.946 | 1.943 | 1.942 |
| $\Delta_d(\text{Ni1})\times 10^4$ | 2.10 | | | |
| Ni2-O1(Å) | 1.960(16) | | | |
| Ni2-O2(Å) | 1.966(15) | | | |
| Ni2-O3(Å) | 2.023(15) | | | |
| ⟨Ni2-O⟩(Å) | 1.983 | | | |
| $\Delta_d(\text{Ni2})\times 10^4$ | 0.71 | | | |
| Ni1-O1-Ni2 | 155.6(9) | 156.5(3) | 157.6(3) | 157.6(3) |
| Ni1-O2a-Ni2 | 161.4(7) | 155.7(8) | 156.1(8) | 156.8(7) |
| Ni1-O2b-Ni2 | 150.6(7) | | | |

$T_{MI}$. The characteristic splitting expected for some reflections in the monoclinic structural distortion was unambiguously confirmed. Figure 4 shows an example of monoclinic doublet observable at 50 K. The splitting of the (40–4)/(404) reflections, as expected in the case of $P2_1/n$ symmetry, is clearly visible and reproduced only with the monoclinic description. Instead of the single (404) reflection appearing in the *Pbnm* symmetry (as observed in the high temperature phase), (40–4)/(404) reflections appear split in the insulating state. The crystal structure of $NdNiO_3$ was thus satisfactorily refined using the same description reported for $YNiO_3$ (Ref. 17). With decreasing temperature, the $b$ parameter in $YNiO_3$ contracts at $T_{MI}(\Delta b/b=-0.16\%)$ and $c$ expands. In $NdNiO_3$, $b$ expands and $a$ contracts decreasing temperature across $T_{MI}$, and as a result $NdNiO_3$ switches from $\mathbf{O''}(a>b>c/\sqrt{2})$ to $\mathbf{O'}(b>a>c/\sqrt{2})$.

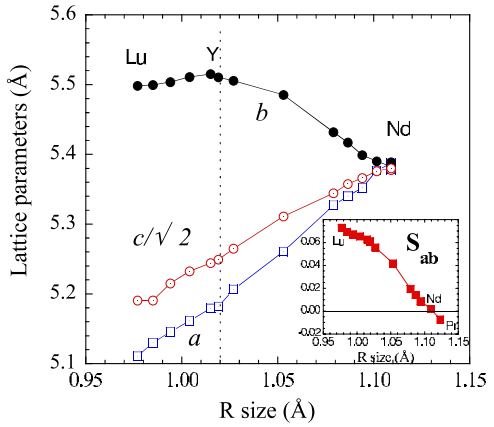


FIG. 2. (Color online) Evolution of cell parameters in $RNiO_3$ perovskites at RT. The figure illustrates the high pseudocubicity of $NdNiO_3$. Inset: evolution of the orthorhombic strain $S_{ab}[S_{ab}=(a-b)/(a+b)]$. (R size: averaged ionic radii of rare-earths at the A-site of the perovskite).

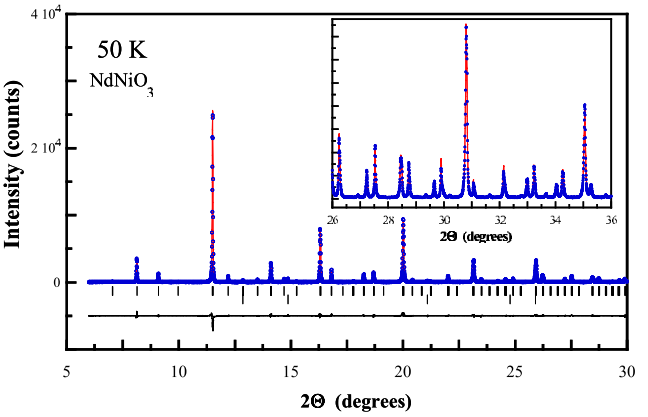


FIG. 3. (Color online) Observed (crosses), calculated (line), and difference synchrotron SPD pattern for $NdNiO_3$ at 50 K using the monoclinic $P2_1/n$ true symmetry. The inset shows the fit of the high-angle region. (Lower ticks correspond to NiO impurity phase.)

The excellent fit using the $P2_1/n$ symmetry establishes the presence of two inequivalent Ni sites. Table I contains the atomic coordinates obtained in the refinements of the insulating phase. The monoclinic angle $\beta=90.069(1)°$ presents a

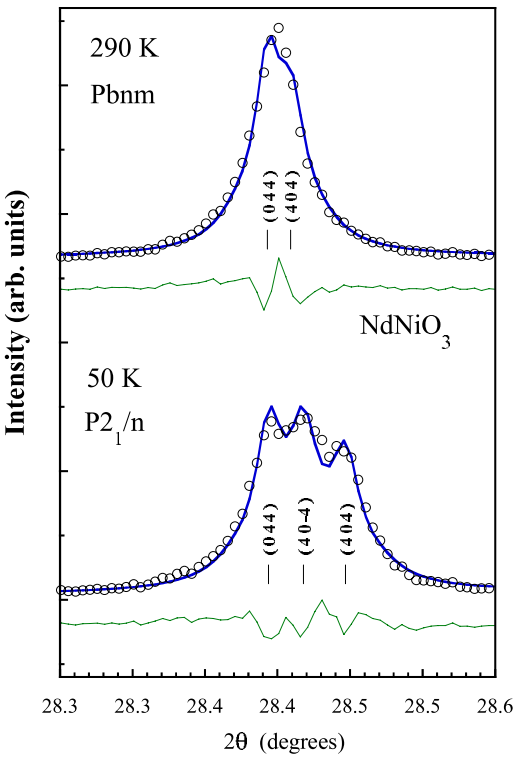


FIG. 4. (Color online) Observed and calculated powder-diffraction intensities around the orthorhombic (044)/(404) pair of reflections. Top: 290 K (metallic, orthorhombic) showing the doublet. Bottom: 50 K (insulating, monoclinic) showing the triplet. Note the (40–4) and (404) monoclinic splitting.

very small deviation from 90°, smaller than any other value previously reported for the heaviest rare-earth nickelates (from $\beta$=90.16° for Lu to $\beta$=90.08° for Ho and Y). Such a small deviation and the strong pseudocubicity of the cell edges made it difficult to determine the correct structure/symmetry of $NdNiO_3$. In present case, the instrumental contribution to the width of the peaks was ~0.003°, neglecting the broadening at low angles due to the axial divergence. Figures 3 and 4 illustrate the excellent agreement between the observed and calculated SPD profile for the insulating low-temperature phase of $NdNiO_3$. Table II contains selected bond distances and angles for the true monoclinic structure.

Table II proves that there are two different octahedral oxygen environments related with two crystallographically independent Ni positions (Ni1 and Ni2 sites). Oxygens breathe in toward Ni1 yielding $\langle$Ni1-O$\rangle$=1.910 Å (contracted), and out of Ni2: $\langle$Ni2-O$\rangle$=1.984 Å (expanded). Both distances are clearly well above and below the average distance beyond $T_{MI}$: 1.943(2) Å. The observed Ni-O bond lengths confirm charge disproportionation/segregation in $NdNiO_3$: $2\ e_g^1 \rightarrow e_g^{1-\delta} + e_g^{1+\delta}$. Ni1 site is electron depleted and Ni2 electron rich. In the ionic limit of the charge order picture Ni1 would correspond to $Ni^{4+}$ and Ni2 to $Ni^{2+}$ sites. The actual structure of the insulating phase of $RNiO_3$ oxides with $T_{IM}=T_N$ was lacking and has been a matter of controversy during the last ten years. Our high-resolution structural study demonstrate long-range charge order in the insulator state for the large rare-earth nickelate $NdNiO_3$.

$LuNiO_3$ is the end member of small $RNiO_3$. The average bond lengths for the two octahedra in $LuNiO_3$ at RT are, respectively, $\langle$Ni1-O$\rangle$=1.9147 Å and $\langle$Ni2-O$\rangle$=1.9990 Å.[18] Their difference, $\Delta d$, for $LuNiO_3$ is $\Delta d$(Lu)=0.084 Å. In $NdNiO_3$ we have obtained $\Delta d$(Nd)=0.072 Å; hence in the present case the difference has been reduced with respect to the smallest nickelates of the family [$\Delta d$(Nd)$<\Delta d$(Lu)]. Therefore, we must conclude that the degree of charge segregation $\delta$ has diminished in $RNiO_3$ on going from small to large lanthanides. Ni valences at Ni1 and Ni2 sites were estimated using the standard approach of Brown's bond-valence model (BVM)[30] ($R_0$=1.686 for the $Ni^{3+}$-$O^{2-}$ pair). The estimated valences are $V_1=+3.27(7)$ for Ni1 sites (expanded) and $V_2=+2.70(7)$ for Ni2 (contracted) [$\delta \approx \delta' \approx 0.28(7)e$]. In Ref. 26 a value of $\delta+\delta' \approx 0.45(4)e$ was estimated from resonant x-ray scattering in an epitaxial film of $NdNiO_3$, also consistent with a diminution of charge segregation.

Moreover, as shown in Table II, the octahedral-site distortion of the two octahedra in $NdNiO_3$ is $\Delta_d(\mathrm{Ni1})=2.1\times10^{-4}$ and $\Delta_d(\mathrm{Ni2})=0.7\times10^{-4}$. As in the case of $LuNiO_3$, the deformation in the octahedra is very small, between 1 and 2 orders of magnitude smaller than in JT $RMnO_3$ compounds ($\Delta_d(LaMnO_3)=33.1\times10^{-4}$). It is thus demonstrated that long-range charge ordering is preferred to Jahn-Teller distortion in antiferromagnetic $NdNiO_3$. Consequently, $NdNiO_3$ should be considered an almost-metallic oxide ($LaNiO_3$ is metallic in all the temperature range), in which partial charge disproportionation (charge order) is energetically favored to Jahn-Teller distortion in spite of the Hubbard repulsion. These results confirm that the model and calculations presented in Ref. 20 also apply to the present case, and $NdNiO_3$, as well as large volume nickelates with $T_{MI}=T_N$, must be considered band insulators below the transition. Despite the hybridized state, the gap opens between essentially the polarized $e_g\uparrow$ band of $Ni^{2+}$ and the roughly unpolarized $e_g$ band of $Ni^{4+}$.[20] The insulating state is stabilized through the energy gained by the contraction (expansion) of $Ni^{3+\delta}O_6$($Ni^{3-\delta}O_6$) octahedra. Long and short Ni-O bonds appear forming a long-range-ordered configuration. Moreover electrons remain partially delocalized. The Hund coupling at the $e_g\uparrow$ band (mainly formed of $Ni^{2+}$ states) overcomes the on site repulsion $U$ at $Ni^{3-\delta}$ sites, which has been reduced thanks to (i) the breathing distortion in the octahedra, and (ii) the Ni-O hybridization favored by a very small or negative $3d$(Ni)-$2p$(O) charge-transfer gap.

In this work we provided the true structure of $NdNiO_3$ in the insulating state (the compound of the family presenting the minimum orthorhombic strain and almost pseudocubic lattice). This is one of the $RNiO_3$ perovskites with largest rare earths, presents a single structural and magnetic transition ($T_N=T_{MI}$) for the onset of antiferromagnetic and charge ordering. Its crystal structure confirms that $NdNiO_3$ presents long-range charge order below $T_{MI}(=T_N)$, with $\delta \approx 0.2-0.3 \ll 1$. The difference between the two Ni-O bond lengths, $\Delta d$=0.072 Å in $NdNiO_3$, is smaller than in the nickelates with smaller rare earths, indicating a diminution of $\delta$. The insulating structure of $NdNiO_3$ confirms that band gap opening and degeneracy lifting in the extreme of the $RNiO_3$ series with larger lanthanides (for which $T_N=T_{MI}$) is driven by the same mechanism as in the heaviest (small) rare-earth nickelates ($T_N \ll T_{MI}$). The whole family of $RNiO_3$ perovskites must be considered band insulators with a charge ordered ground state at low temperature. The only exception is $LaNiO_3$, in which the higher hybridization between adjacent Ni sites avoids both Jahn-Teller effect but also charge segregation.

Financial support from MICINN (Spanish government) under Projects No. MAT2006-11080-C02-02, No. MAT2007-60536, and NANOSELECT Grant No. CSD2007-00041, and Generalitat de Catalunya (Grant No. 2005-GRQ-00509) is thanked. We thank European Synchrotron Radiation Facility for the provision of beam time. The FAME European Network of Excellence is also acknowledged.

*Corresponding author; garcia.munoz@icmab.es

[1] P. Lacorre, J. B. Torrance, J. Pannetier, A. I. Nazzal, P. W. Wang, and T. C. Huang, J. Solid State Chem. **91**, 225 (1991).

[2] J. B. Torrance, P. Lacorre, A. I. Nazzal, E. J. Ansaldo, and Ch. Niedermayer, Phys. Rev. B **45**, 8209 (1992).

[3] J. L. Garcia-Munoz, J. Rodriguez-Carvajal, P. Lacorre, and J. B. Torrance, Phys. Rev. B **46**, 4414 (1992).

[4] M. Medarde, P. Lacorre, K. Conder, F. Fauth, and A. Furrer,

Phys. Rev. Lett. **80**, 2397 (1998).
[5] J. L. García-Muñoz, J. Rodríguez-Carvajal, and P. Lacorre, Europhys. Lett. **20**, 241 (1992).
[6] J. L. García-Muñoz, J. Rodríguez-Carvajal, and P. Lacorre, Phys. Rev. B **50**, 978 (1994).
[7] J. L. García-Muñoz, P. Lacorre, and R. Cywinski, Phys. Rev. B **51**, 15197 (1995).
[8] M. T. Fernández-Díaz, J. A. Alonso, M. J. Martínez-Lope, M. T. Casais, and J. L. García-Muñoz, Phys. Rev. B **64**, 144417 (2001).
[9] J. Rodríguez-Carvajal, S. Rosenkranz, M. Medarde, P. Lacorre, M. T. Fernández-Díaz, F. Fauth, and V. Trounov, Phys. Rev. B **57**, 456 (1998).
[10] J. S. Zhou, J. B. Goodenough, B. Dabrowski, P. W. Klamut, and Z. Bukowski, Phys. Rev. Lett. **84**, 526 (2000).
[11] J. S. Zhou and J. B. Goodenough, Phys. Rev. B **69**, 153105 (2004).
[12] J. A. Alonso, M. J. Martínez-Lope, M. T. Casais, J. L. Martínez, G. Demazeau, A. Largeteau, J. L. García-Muñoz, A. Muñoz, and M. T. Fernández-Díaz, Chem. Mater. **11**, 2463 (1999).
[13] J. S. Zhou, J. B. Goodenough, and B. Dabrowski, Phys. Rev. Lett. **95**, 127204 (2005).
[14] J. S. Zhou, J. B. Goodenough, and B. Dabrowski, Phys. Rev. Lett. **94**, 226602 (2005).
[15] J. L. García-Muñoz, M. Amboage, M. Hanfland, J. A. Alonso, M. J. Martínez-Lope, and R. Mortimer, Phys. Rev. B **69**, 094106 (2004).
[16] V. Scagnoli, U. Staub, A. M. Mulders, M. Janousch, G. I. Meijer, G. Hammerl, J. M. Tonnerre, and N. Stojic, Phys. Rev. B **73**, 100409(R) (2006).
[17] J. A. Alonso, J. L. García-Muñoz, M. T. Fernández-Díaz, M. A. G. Aranda, M. J. Martínez-Lope, and M. T. Casais, Phys. Rev. Lett. **82**, 3871 (1999).
[18] J. A. Alonso, M. J. Martínez-Lope, M. T. Casais, J. L. García-Muñoz, and M. T. Fernández-Díaz, Phys. Rev. B **61**, 1756 (2000).
[19] J. A. Alonso, M. J. Martínez-Lope, M. T. Casais, J. L. García-Muñoz, M. T. Fernández-Díaz, and M. A. G. Aranda, Phys. Rev. B **64**, 094102 (2001).
[20] I. I. Mazin, D. I. Khomskii, R. Lengsdorf, J. A. Alonso, W. G. Marshall, R. M. Ibberson, A. Podlesnyak, M. J. Martínez-Lope, and M. M. Abd-Elmeguid, Phys. Rev. Lett. **98**, 176406 (2007).
[21] E. Wawrzynska, R. Coldea, E. M. Wheeler, I. I. Mazin, M. D. Johannes, T. Sorgel, M. Jansen, R. M. Ibberson, and P. G. Radaelli, Phys. Rev. Lett. **99**, 157204 (2007).
[22] I. Vobornik, L. Perfetti, M. Zacchigna, M. Grioni, G. Margaritondo, J. Mesot, M. Medarde, and P. Lacorre, Phys. Rev. B **60**, R8426 (1999).
[23] K. Okazaki, T. Mizokawa, A. Fujimori, E. V. Sampathkumaran, M. J. Martinez-Lope, and J. A. Alonso, Phys. Rev. B **67**, 073101 (2003).
[24] I. V. Nikulin, M. A. Novojilov, A. R. Kaul, A. F. Maiorova, and S. N. Mudretsova, Mater. Res. Bull. **39**, 803 (2004).
[25] M. Zaghrioui, A. Bulou, P. Lacorre, and P. Laffez, Phys. Rev. B **64**, 081102(R) (2001).
[26] U. Staub, G. I. Meijer, F. Fauth, R. Allenspach, J. G. Bednorz, J. Karpinski, S. M. Kazakov, L. Paolasini, and F. d'Acapito, Phys. Rev. Lett. **88**, 126402 (2002).
[27] C. Piamonteze, H. C. N. Tolentino, A. Y. Ramos, N. E. Massa, J. A. Alonso, M. J. Martínez-Lope, and M. T. Casais, Phys. Rev. B **71**, 012104 (2005).
[28] J. A. Alonso, M. J. Martinez-lope, and M. Hidalgo, J. Solid State Chem. **116**, 146 (1995).
[29] J. Rodríguez-Carvajal, Physica B **55**, 192 (1993).
[30] I. D. Brown, Z. Kristallogr. **199**, 255 (1992).